

Article

Evolution of the Anisotropic Thermal Conductivity of Oil Shale with Temperature and Its Relationship with Anisotropic Pore Structure Evolution

Juan Jin ^{1,2}, Jiandong Liu ^{1,2,*}, Weidong Jiang ^{1,2}, Wei Cheng ^{1,2} and Xiaowen Zhang ^{1,2}¹ Research Institute of Petroleum Exploration & Development, PetroChina, Beijing 100083, China² Key Laboratory of Oil & Gas Production, CNPC, Beijing 100083, China

* Correspondence: liuscienceoil@163.com

Abstract: Due to its sedimentary characteristics and natural fractures, oil shale shows anisotropy in heat transfer characteristics. Moreover, the anisotropic thermal conductivity will change with the temperature. This change in the anisotropic thermal conductivity coefficient affects the temperature field distribution and heating efficiency during the in situ electric heating pyrolysis of oil shale. Therefore, it is very important to study the evolution of the anisotropy thermal conductivity coefficient of oil shale with temperature. In this study, the variation of weight loss and the specific heat of an oil shale with temperature is investigated using a differential scanning calorimeter. The variation of the anisotropic pore and fracture structure of the oil shale with temperature is studied through CT scanning technology. The variation of the anisotropic thermal conductivity with temperature is studied through the hot disk method. Finally, the relationship between the change in the anisotropic heat conductivity of the oil shale and the evolution of the anisotropic pore and fracture structure is discussed. The results show that the mass loss of oil shale mainly occurs after 400 °C. The thermal conductivity of both perpendicular and parallel to bedding directions decreases linearly with the increase of temperature. The research results of this study can serve as an important reference in the study of the in situ pyrolysis of oil shale.

Keywords: high temperature; thermal conductivity; pore and fracture; anisotropy; oil shale



Citation: Jin, J.; Liu, J.; Jiang, W.; Cheng, W.; Zhang, X. Evolution of the Anisotropic Thermal Conductivity of Oil Shale with Temperature and Its Relationship with Anisotropic Pore Structure Evolution. *Energies* **2022**, *15*, 8021. <https://doi.org/10.3390/en15218021>

Academic Editor: Reza Rezaee

Received: 6 September 2022

Accepted: 3 October 2022

Published: 28 October 2022

Publisher's Note: MDPI stays neutral with regard to jurisdictional claims in published maps and institutional affiliations.



Copyright: © 2022 by the authors. Licensee MDPI, Basel, Switzerland. This article is an open access article distributed under the terms and conditions of the Creative Commons Attribution (CC BY) license (<https://creativecommons.org/licenses/by/4.0/>).

1. Introduction

Oil shale has an obvious bedding structure and is rich in organic matter, which can be pyrolyzed into pyrolysis oil and gas at a high temperature. Therefore, oil shale is considered as an important alternative energy for traditional oil resources and is widely distributed in the world, with about 4.8 trillion bars of reserves [1–3]. China is rich in oil shale resources, which are mainly distributed in Jilin, Liaoning, Guangdong, Shandong, Xinjiang, Inner Mongolia, and other provinces. China's estimated oil shale resources are about 720 billion tons, which is convertible into shale oil resources of about 47.6 billion tons, making it rank second in the world; this amount also exceeds China's total cumulative proven natural oil reserves [4–6].

At present, the world's mainstream oil shale mining methods include ground retorting and in situ pyrolysis [7,8]. However, due to its small output and prominent environmental pollution problems, reserves obtained from ground-retorting technology cannot compete with those obtained from conventional oil, but they are an alternative oil energy resource [9–11]. Compared with ground-retorting technology, in situ mining of oil shale has the characteristics of environmental friendliness, high efficiency, and economical extraction. Oil shale in situ mining technology has attracted the attention of researchers from all over the world and is classified into solid-heating technology (such as Shell's ICP technology) and fluid-heating technology (such as Chevron's CRUSH technology). Among them, the

heat conduction through solid-heating technology mainly depends on the thermal conductivity of the oil shale itself and, therefore, it is very important to study the thermal conductivity of oil shale at different temperatures (Figure 1).

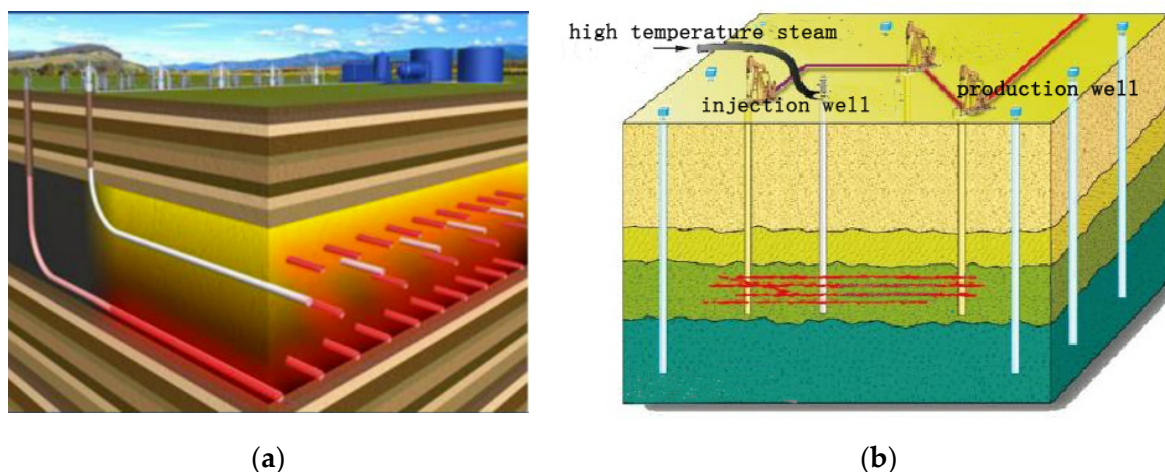


Figure 1. Schematic diagram of in situ heating oil shale technology. (a) ICP electric heating technology [12]; (b) Chevron crush technology [13]. (Lonney et al. 2011).

However, the ordered arrangement and special sedimentary structure of oil shale minerals result in obvious anisotropy in many aspects, such as physical characteristics, mechanical characteristics, permeability characteristics, and so on [14–16]. For example, flat minerals such as clay minerals tend to be oriented parallel to the bedding direction. The arrangement of such minerals forms a natural barrier to fluid flow in the direction of perpendicular to beddings, resulting in low thermal conductivity in the direction of perpendicular to beddings (K_{per}). The natural weak surface formed in the deposition process, and the existence of microcracks, prevents the transfer of heat in the direction of perpendicular to beddings. Therefore, the existence of microcracks and mineral arrangements causes an anisotropy of heat conduction characteristics. The anisotropic thermal conductivity of oil shale affects the heat conduction in the oil shale deposit, and then this affects the prediction of the temperature conduction range and the heating efficiency [17–19].

To date, many scholars have studied the variation of rock thermal conductivity with temperature and have found that thermal conductivity decreases when the temperature increases [20–24]. Under the action of temperature, the mass loss of the mineral composition, the expansion of internal microcracks, and the increase in the pores decrease the heat conductivity [25–27]. However, unlike other rocks, oil shale is rich in organic matter and will decompose with an increase in temperature. Due to the difference in the composition of oil shale in different regions, the sensitivity of the thermophysical characteristics of the different oil shales to temperature is also different. Li [28] performed an in-depth study of the thermophysical parameters of oil shale in the Huadian area. The results showed that the specific heat capacity decreased when the pretreatment temperature increased; the thermal conductivity increased from normal temperature to 150 °C and then decreased gradually. The thermal diffusion coefficient first increased, then decreased, and then increased again. The changes in these parameters were affected by the porosity, water content, and organic matter precipitation of the oil shale samples. The results show that the thermal conductivity parallel to the beddings (K_{par}) is 1.07~1.09 times that perpendicular to the bedding direction. Wang [29] studied the change in the thermophysical properties of oil shale in the Huadian area during heating. The results show that the thermal conductivity and specific heat capacity of the oil shale increase when the temperature increases from normal temperature to 150 °C; in the stage of 150–520 °C, the thermal conductivity and specific heat capacity decreased when the temperature increased; at 520–750 °C, the thermal conductivity and specific heat capacity basically remained unchanged with the increase in temperature.

Zhou [30] studied the Nong'an oil shale and found that the K_{par} and K_{per} had a good consistency with the change in the temperature. However, K_{per} was larger, indicating that it had anisotropic characteristics. This characteristic is related to the bedding structure of oil shale. During the deposition process, the vertical stress of the oil shale is less than the horizontal stress and, therefore, the compactness in the vertical bedding direction is poor. The thermal conductivity is directly proportional to the compactness of the rock and, therefore, the thermal conductivity is small in the vertical bedding direction [31].

A large number of scholars have studied the development of pore fractures in oil shale under high temperatures. Kang [32] studied the thermal fracture characteristics of Fushun oil shale using CT scanning technology and found that the thermal fracture of oil shale before 300 °C is mainly caused by thermal stress, while the thermal fracture after 300 °C is mainly caused by the decomposition of organic matter. However, it is not clear what kind of mineral causes the thermal stress and the contribution of organic matter pyrolysis to thermal cracking. Saif et al. [33] studied the evolution law of pores and fractures in Green River oil shale by using CT scanning technology and found that the temperature point of rapid development of pores and fractures is about 400 °C and the amount of organic matter content has a great impact on porosity. Sun et al. [2] used a variety of experimental methods to study the thermal effect and physical and chemical characteristics of oil shale. The 100~800 °C pyrolysis experiment of the Huadian oil shale shows that temperature has a great influence on the yield of pyrolysis products and the change of pore structure; 350~500 °C is the main stage of kerogen decomposition and the smaller the pore, the more complex the structure.

In this study, the change in the weight and specific heat of an oil shale with temperature is studied using a differential scanning calorimeter, the variation of the anisotropic pore structure and the fracture structure of the oil shale with temperature is investigated by CT scanning technology, and the change in the anisotropic heat conductivity with temperature is investigated using the hot disk method. Finally, the relationship between the change in the anisotropic heat conductivity of the oil shale and the evolution of the anisotropic pore fissure structure is discussed. The research results of this study can serve as an important reference in the study of the in situ heating and oil production of shale.

2. Experimental Equipment and Experimental Procedures

2.1. Preparation of Test Pieces

(a) Test specimen for the specific heat capacity measurements: irregular-shaped samples can be used as oil shale samples. Six samples were chosen and they were heated to 200 °C, 300 °C, 400 °C, 500 °C, and 600 °C, respectively, and then cooled to room temperature. Then, the specific heat capacity of the oil shale samples subject to different temperatures was tested to avoid the influence of kerogen decomposition and heat absorption in the oil shale on the specific heat capacity of the oil shale matrix. The oil shale test specimens used for the specific heat measurements are shown in Figure 2.

(b) Test specimens for the pore and fracture measurements: cylindrical oil shale samples with a size of $\Phi 10 \text{ mm} \times 15 \text{ mm}$ were pyrolyzed at 200 °C, 300 °C, 400 °C, 500 °C, and 600 °C, respectively, and then cooled for the CT scanning experiment.

(c) Test specimens for the thermal conductivity measurements: the oil shale samples were processed into thin squares with sizes of $20 \times 20 \times 1 \text{ mm}$ [32] and the thickness direction of the specimens was the direction of the tested thermal conductivity. The specimens were divided into two groups: the specimens whose thermal conductivity direction was processed parallel to the oil shale bedding plane were marked as parallel bedding direction specimens and the specimens whose thermal conductivity direction was processed perpendicular to the oil shale bedding plane were marked as vertical layer specimens. As shown in Figure 3, each group of test pieces was processed several times, and 6 test pieces with more regular grinding planes were selected for the test, as shown in Figure 4.

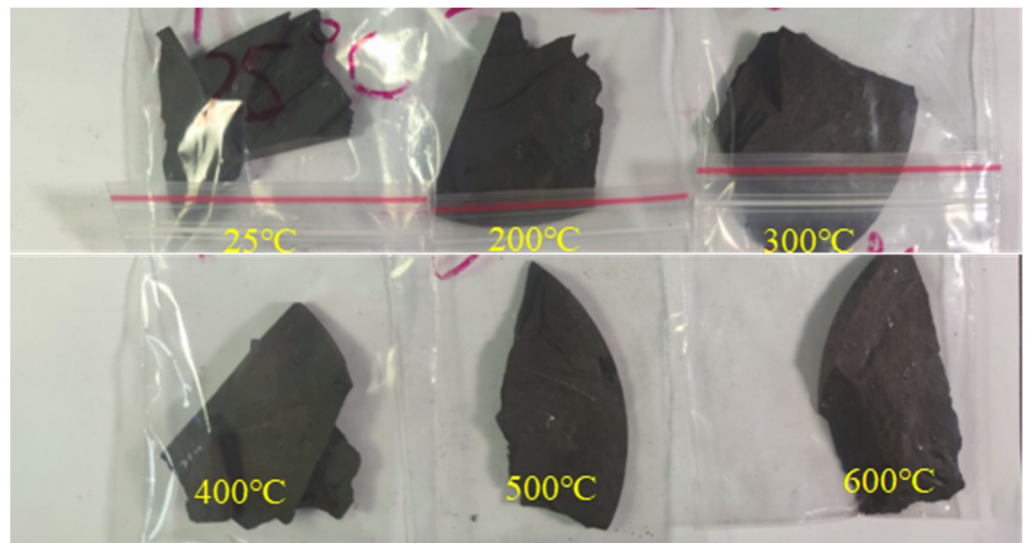


Figure 2. Specific heat test specimen.

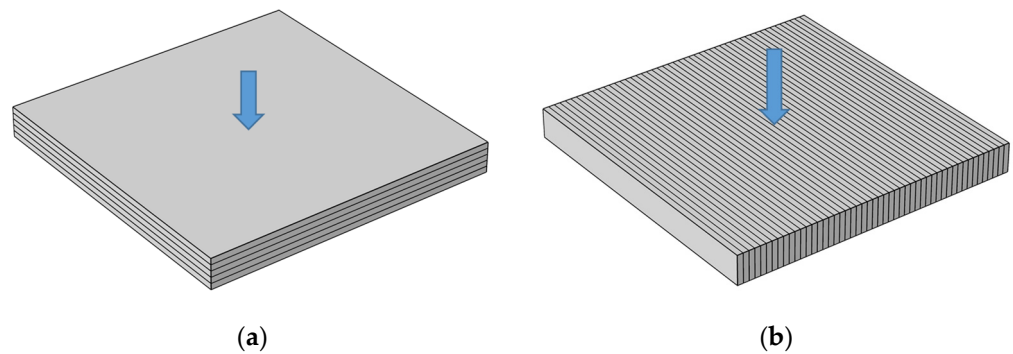


Figure 3. Schematic diagram of the heat conduction direction [32]. (a) Perpendicular to bedding; (b) parallel to bedding. (Yu et al. 2015 [31]).

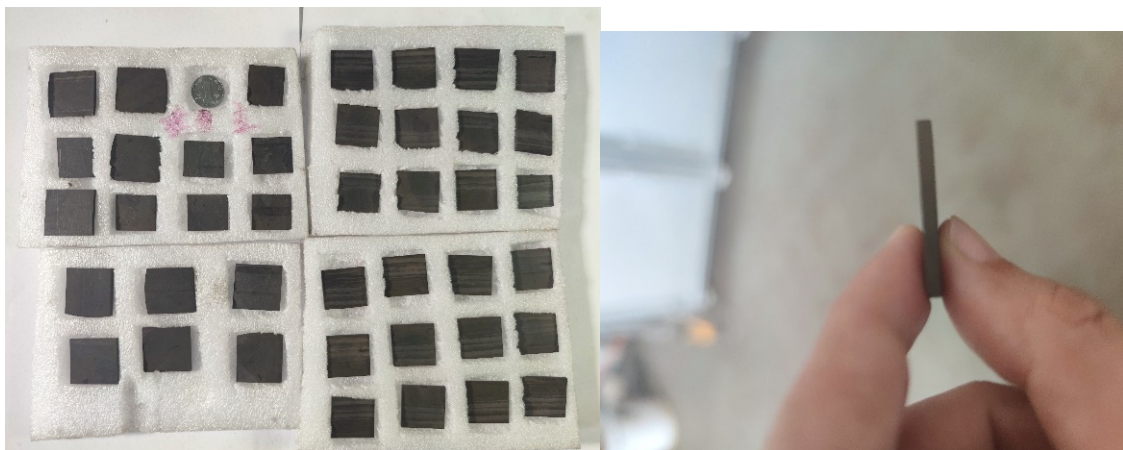


Figure 4. Oil shale test specimen [29].

2.2. Experimental Equipment and Procedures

(a) Thermogravimetric experiment: thermogravimetric analysis of the oil shale was carried out using a STA 449F3 (Netzsch, Bavaria, Germany) thermal analyzer (Figure 5a). The specimen was heated to 600 °C at a heating rate of 10 °C/min, and nitrogen protection with a nitrogen flow rate of 50 mL·min⁻¹ was passed during the heating process.

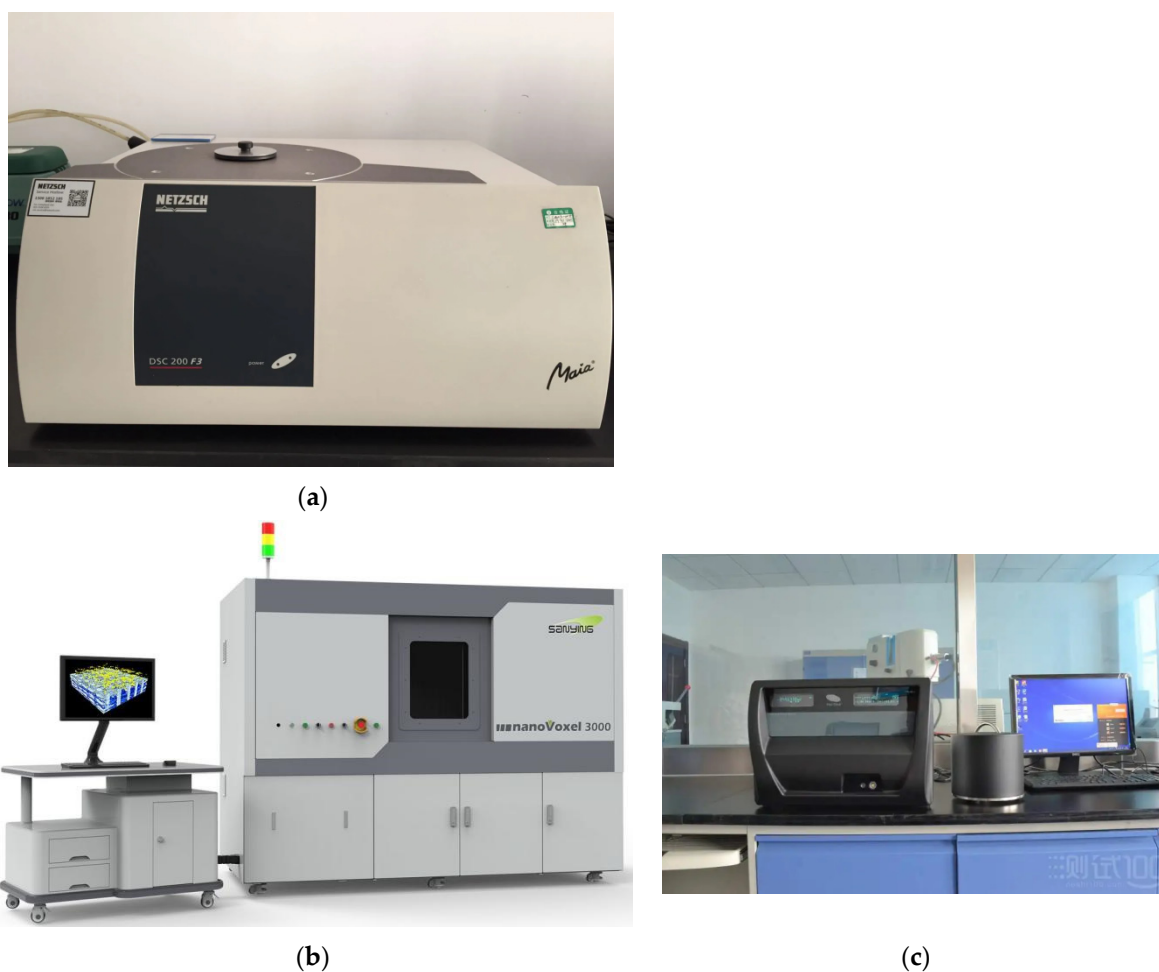


Figure 5. Experimental equipment [34]. (a) Differential scanning calorimeter; (b) NanoVoxel-3502E CT scanner; (c) hot disk thermal constant analyzer. (Wang et al. 2018).

(b) Specific heat experiment: the DSC-200-F3 (Netzsch, Germany, bavaria) differential scanning calorimeter (Figure 5b), produced by NETZSCH, Germany, was used to test the evolution of the specific heat capacity of the oil shale with temperature. The heated oil shale specimen was placed in the sample furnace, heated to the preset temperature of 200 °C, 300 °C, 400 °C, 500 °C, and 600 °C, and the specific heat capacity of the oil shale specimens was tested.

(c) Pore and fracture test experiment: the specimens were placed on the working turntable of a nanoVoxel-3502E high-resolution X-ray 3D CT scanner (Sanying Precision Instrument Co., Ltd., Tianjin China) (Figure 5b) (and non-destructive CT scans with a spatial resolution of 6.5 μm were performed in sequence. Before scanning, the cylindrical specimen was placed vertically in the center of the micro-CT scanning table and the specimen was corrected to the center of the scanning area by adjusting the height of the fixture. Then, the scanning parameters of the instrument were adjusted according to the size of the specimen and a high-definition resolution of the scanned image was ensured by adjusting the current and voltage. After adjusting the parameters, the test piece was scanned once for every 0.9° rotation of the turntable, generating a total of 1400 images.

(d) Thermal conductivity test experiment: the thermal conductivity test was performed using a hot disk thermal constant analyzer (Figure 5c). The sample was placed according to the physical model of the selected test module, and the contact time between the finger and the sample was minimized during the placement process to reduce the heat transfer from the human body to the sample. After the sample was placed, it was made to stand for 20 min at room temperature until the internal temperature distribution of the

sample reached a stable state to prevent heat transfer caused by the difference between the sample's temperature and the ambient temperature.

3. Experimental Results

3.1. Oil Shale Weight Loss at Different Temperatures

Figure 6 shows the TG and DTG curves of the oil shale sample. Based on these curves, the pyrolysis of the oil shale can be divided into the following three stages:

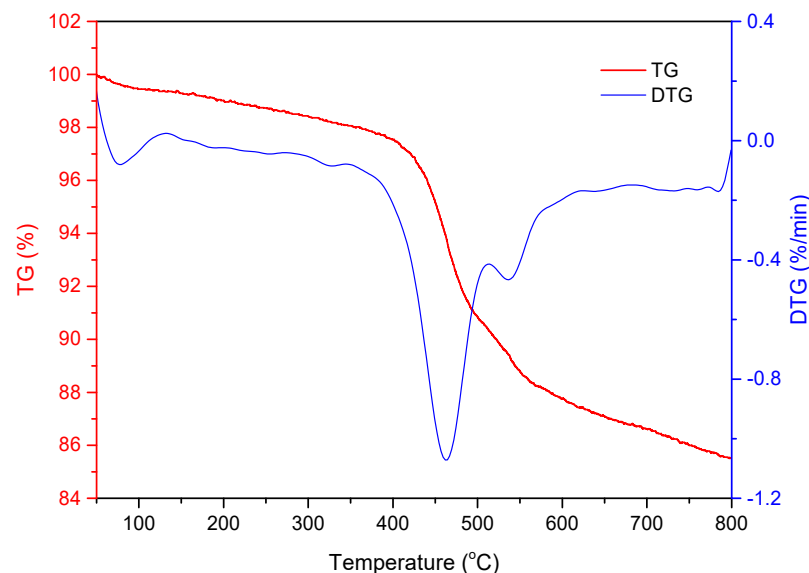


Figure 6. TG and DTG curves of the weight loss during oil shale pyrolysis. TG—thermogravimetry. DTG—differential thermogravimetric.

(1) Low-temperature weight loss stage, from room temperature to 350 °C

The weight loss at this stage is mainly caused by the precipitation of water, including the structural water and the interlayer water of the clay minerals. The weight loss at this stage is about 2% of the total weight loss. At this stage, the TG curve declines, the DTG curve is at 150 An, and an obvious peak of water loss appears before 150 °C.

(2) Medium temperature weight loss stage, 350~580 °C

In this temperature range, the oil shale has the characteristics of centralized pyrolysis and its weight loss is very large, accounting for about 12% of the total weight loss. This is due to the large amount of pyrolysis of the organic matter in the oil shale, resulting in a large amount of shale oil and a large number of gaseous products. At this stage, the TG curve shows a large decline and a large peak appears on the DTG curve.

(3) High-temperature weight loss stage, 580~800 °C

This stage is generally considered to be the cracking stage of carbonates such as calcite and dolomite. In addition, the fixed carbon contained in the oil shale leads to high-temperature carbonization and the carbonaceous particles disintegrate due to heating, producing a small amount of volatile gas and causing a certain amount of thermal weight loss. The TG curve shows a decline and the weight loss accounts for about 3% of the total weight loss. The DTG curve is not very obvious.

3.2. Variation of the Anisotropic Pore and Fracture Structure at Different Temperatures

Figure 7 shows the structural evolution characteristics of the oil shale at different positions in the XZ direction (vertical bedding) at different temperatures. It can be seen that with the rise in temperature, the evolution characteristics of the pore fissure structure of the oil shale can be divided into the following temperature stages.

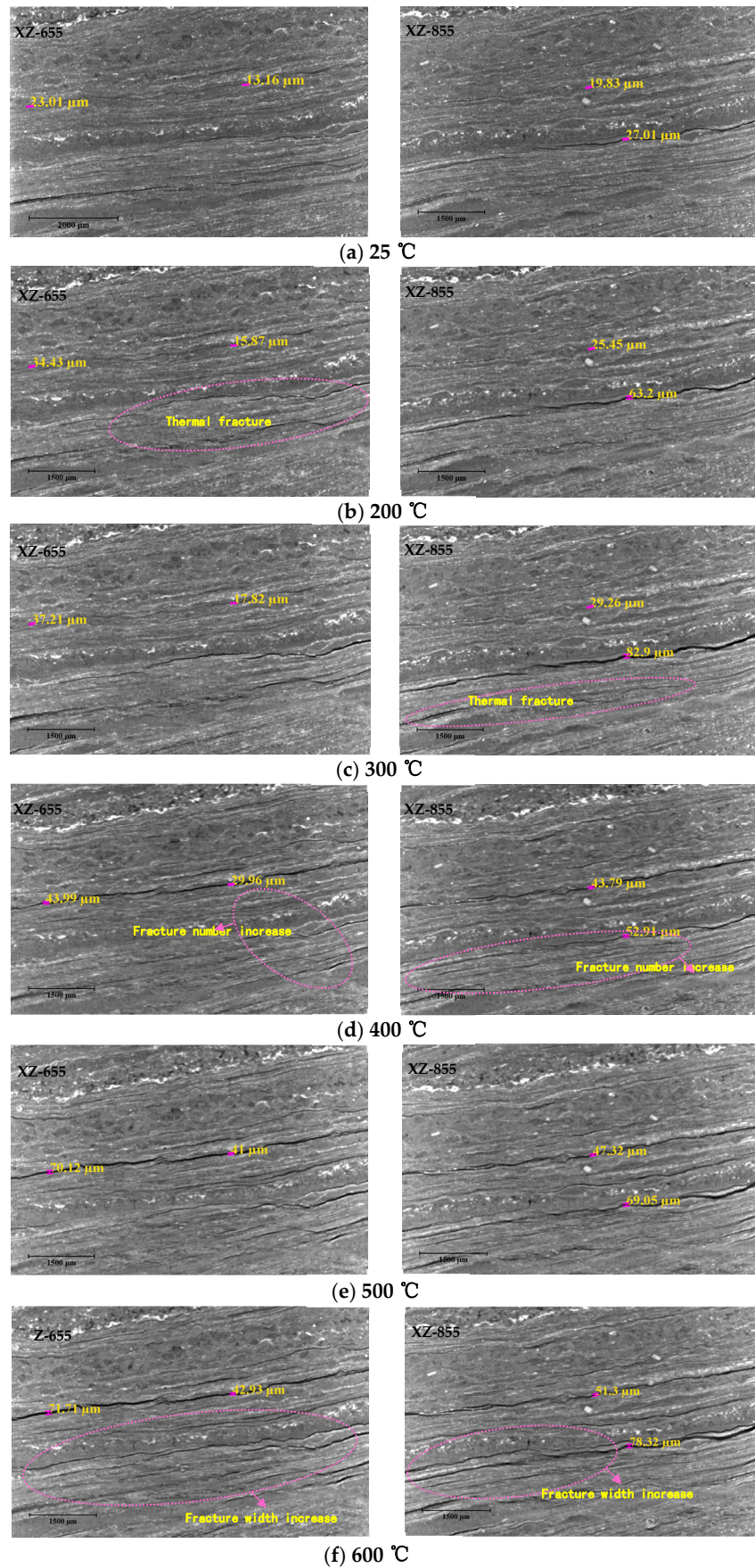


Figure 7. Structural evolution of the oil shale at different positions in the XZ direction at different temperatures.

(1) 20~300 °C

It can be seen from Figure 7 that the oil shale is relatively dense at room temperature, showing significant sedimentary characteristics of argillaceous and sandy interbedding, and the argillaceous layer deposition is grayish-black overall and the sandy layer is gray–white overall. Under the original condition, there are a few original fracture structures parallel to the bedding in the oil shale; these are at the junction of the argillaceous layer and the sandy layer, and the fracture width is basically 10~30 μm . These cracks prevent temperature conduction along the vertical bedding direction, resulting in poor thermal conductivity in the vertical bedding direction. As the temperature rises to 200 °C and 300 °C, a small number of thermal fracture cracks caused by the uneven thermal expansion of the rock mineral particles are produced in the oil shale (see Figure 7c). At the same time, the width and length of the original cracks are further expanded. At 300 °C, the width range of the original cracks increases to 15~90 μm . At this time, the increase of fracture number and fracture opening is mainly related to the evaporation of free water and adsorbed water in oil shale.

(2) 300~400 °C

At the temperature rise stage of 300 to 400 °C, some light organic substances in the oil shale undergo significant thermal decomposition reactions to generate shale oil and gas, as shown in Figure 6. After the pyrolysis of the much banded organic matter, a large number of fracture structures with various levels parallel to the bedding direction are formed in their original location. The formation and development of the large number of new cracks inflates and squeezes the surrounding rocks, resulting in a significant “condensation effect” on the original crack structure, which significantly reduces its opening, as shown in Figure 7c,d. The width of the original crack increases from 80% at 300 °C 80 μm condensed to 30 μm . According to Wang’s research, it is also found that when the temperature rises to 400 °C, the crack width of oil shale also decreases. However, Wang’s research focuses more on the relationship between fracture width and permeability.

(3) 400~600 °C

In the heating stage from 400 to 600 °C, the residual organic matter is further pyrolyzed, as shown in Figure 6, resulting in a qualitative change in the fracture scale inside the oil shale. Cracks parallel to the bedding direction are produced in all parts of the specimen; the number of these cracks is significantly increased and so are their lengths and widths. The original cracks are also widened and extended in this temperature range and the cracks overlap and cross each other. A complex pore fissure connection network structure is formed in the oil shale, which fundamentally reduces the thermal conductivity of the oil shale.

It can be seen that in the range of 300~500 °C, the chemical thermal decomposition reaction of the organic matter dominates the formation process of the pore fissure structure of the oil shale, and the fissures show the characteristics of centralized explosion and extensive development, which makes the originally dense oil shale become a multi fissure and porous medium, resulting in a decline in its thermal conductivity.

3.3. Variation of the Anisotropic Thermal Conductivity of the Oil Shale with Temperature

Figure 8 shows the variation of the thermal conductivity of the oil shale in the vertical bedding and parallel bedding directions with temperature. The measured thermal conductivity of each group of specimens decreases with the increase in temperature, and it has a good linear relationship with temperature. In addition, Figure 8 shows that the thermal conductivity of the oil shale along the direction parallel to the bedding is significantly greater than that along the direction perpendicular to the bedding at the same temperature. According to the heat transfer theory, except for gas mediums, the thermal conductivity of most solids and liquids maintains an approximately linear decreasing trend with temperature and, overall, the thermal conductivity of solids is greater than that of liquids at the same temperature, while the thermal conductivity of liquids is slightly greater than that of gases. Therefore, the

results of this test also roughly conform to this classical heat transfer law. The relationship between thermal conductivity and temperature can be expressed as follows:

$$\lambda_{par} = -0.0007T + 0.9355 \quad (1)$$

$$\lambda_{per} = -0.0006T + 0.8126 \quad (2)$$

Here, T is the temperature, °C; λ_{par} is the thermal conductivity along the parallel bedding, W/(m·K); λ_{per} is the thermal conductivity along the vertical bedding, W/(m·K).

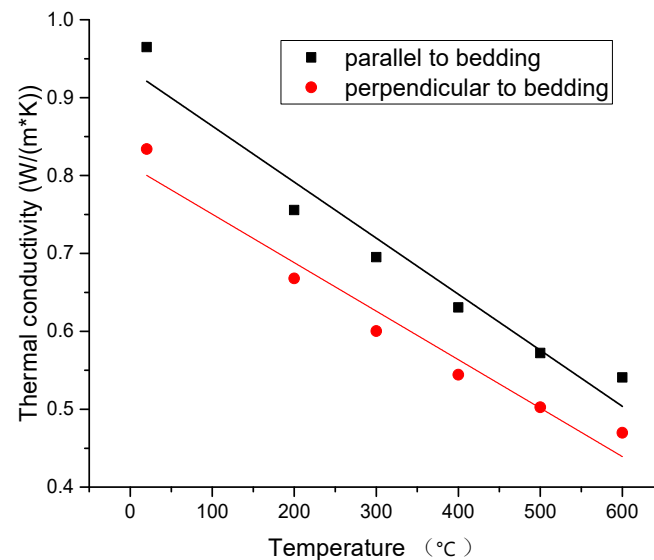


Figure 8. Variation of heat conductivity with temperature.

As the temperature increases, the oil shale begins to slowly undergo phase transition, pyrolysis, and cracking at medium and low temperatures, and the organic matter in it begins to decompose to generate liquid shale oil and hydrocarbon gas. The continuously generated oil and gas weaken the solid framework. Its own thermal conductivity, therefore, shows a decreasing trend with the increase in temperature. In particular, in specimens that conduct heat along the vertical bedding direction, since the heat transfer process passes through the bedding vertically, the primary fractures between the beddings contain moisture or gas, the thermal conductivity of moisture and gas is smaller than that of the rock, and the thermal conductivity obtained along the vertical bedding direction is lower. On the contrary, in specimens that conduct heat along the parallel bedding direction, the parallel bedding oil shale framework is not split by the pyrolysis cracks and the heat transfer process is always in the parallel bedding direction and the heat conduction is carried out in a relatively continuous and solid oil shale framework and, therefore, the obtained thermal conductivity is relatively high.

It can be seen in Figure 8 that the thermal conductivity of the oil shale in the horizontal bedding direction is greater than that in the vertical bedding direction, indicating that it has the characteristics of anisotropy. This characteristic is related to the bedding structure of the oil shale. During the deposition process, due to the shallow burial depth, the vertical stress on the oil shale is smaller than the horizontal stress and, therefore, the compactness in the vertical bedding direction is poor. The thermal conductivity is positively correlated to the compactness of the rock. The anisotropy of the thermal conductivity of the oil shale is represented by the anisotropy coefficient ($\lambda_{par}/\lambda_{per}$) and its variation curve with temperature is shown in Figure 9. It can be seen in Figure 9 that the anisotropy coefficient of the thermal conductivity of the oil shale is between 1.13 and 1.15, indicating that the thermal conductivity in the parallel bedding direction is greater than that in the vertical bedding direction at different temperatures. However, the anisotropy coefficient does not change much with temperature.

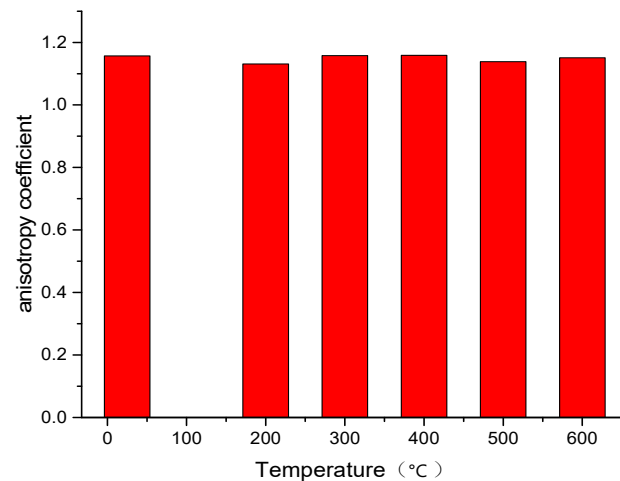


Figure 9. Anisotropy coefficient of the thermal conductivity of the oil shale.

3.4. Variation of the Specific Heat Capacity of the Oil Shale with Temperature

Figure 10 shows that the specific heat of the oil shale first increases and then decreases with the increase in temperature. The average specific heat capacity at room temperature is 1.109 J/(g·K). After the oil shale is heated to a temperature of 200 °C, the specific heat capacity of the oil shale drops to 0.9771 J/(g·K), which is lower than that of the oil shale at room temperature. This is because, after the oil shale is heated to a temperature of 200 °C, the free water and bound water evaporate, resulting in a decrease in the specific heat capacity of the oil shale. When the oil shale is subjected to a high temperature of 300 °C, the specific heat capacity of the oil shale increases as compared with the specific heat capacity at room temperature and 200 °C. This is because the volatile matter inside the oil shale begins to volatilize and absorb heat after 300 °C, increasing the specific heat capacity of the oil shale. When the oil shale is subjected to a high temperature of 400 °C, the specific heat capacity begins to rise sharply at 400 °C, because the kerogen in the 400 °C oil shale begins to undergo a large amount of pyrolysis and absorbs a lot of heat. However, after the oil shale is subjected to a high temperature of 500 °C, the kerogen inside the oil shale has already been pyrolyzed to a large extent, and the specific heat capacity at this time is lower than that at 400 °C. When the temperature is increased again, the internal residual organic matter continues to decompose and the specific heat capacity at 600 °C increases slightly.

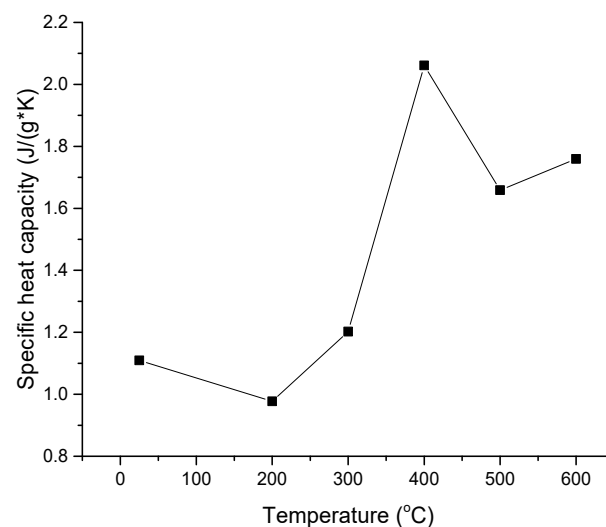


Figure 10. Variation of the specific heat capacity of the oil shale with temperature.

4. Discussion

4.1. Relationship between Thermal Conductivity Evolution and Thermal Cracking

First, the reason why the thermal conductivity along the vertical bedding decreases linearly with temperature is explained. Figure 7 shows the structural evolution characteristics of the oil shale at different temperatures in the XZ direction (vertical bedding) at different positions. It can be seen in the figure that there are many microscopic fractures in the oil shale at room temperature. At room temperature $-300\text{ }^{\circ}\text{C}$, these microscopic fractures make the oil shale more likely to expand in the vertical bedding direction, so that the thermal conductivity continues to decrease with the increase in temperature. According to Yu [30], the thermal expansion deformation of oil shale increases linearly at room temperature $-300\text{ }^{\circ}\text{C}$ under unconstrained conditions, which corresponds to the linear decrease in the thermal conductivity of the oil shale in this project at room temperature $-300\text{ }^{\circ}\text{C}$. As the temperature continues to increase, the softening and swelling deformation of the oil shale is not so obvious. In addition, at room temperature $-300\text{ }^{\circ}\text{C}$, the water in the primary pores and fissures of the oil shale volatilizes, leaving air components, and the poor thermal conductivity of the air also leads to a decrease in the thermal conductivity along the vertical bedding. However, after $400\text{ }^{\circ}\text{C}$, the kerogen in the oil shale begins to decompose in large quantities, and the oil and gas expansion generated by the rapid decomposition of the kerogen generates local high pressure, which leads to the formation of large fractures in weak layers, as shown in Figure 7d–f, resulting in a linear decrease in the thermal conductivity.

The reason for the decrease in the thermal conductivity with temperature along the parallel bedding is explained as follows. It can be seen in Figure 7 that the oil shale is relatively dense at room temperature and the interior is characterized by interbedded argillaceous and sandy deposits. The sandy layer is generally grayish-white, and hard mineral particles (white bright spots in Figure 7, such as quartz and pyrite, etc.) are scattered inside the sandy layer. In each part, the structure is very dense. It can be seen in Figure 7 that the distribution of the hard minerals and the argillaceous minerals in the oil shale is orderly. The thermal conductivity decrease in the parallel bedding direction is less affected by the bedding fractures, and the linear expansion of the oil shale in the parallel bedding direction is larger. Soft mudstone mainly exists between the beddings. Hard minerals affect the thermal expansion in the direction parallel to the bedding. These hard minerals continue to expand and the thermal conductivity in the direction parallel to the bedding continues to decrease linearly.

Figure 11 shows the relationship between the thermal conductivity and porosity. It can be seen in Figure 12a that the thermal conductivity along the vertical bedding and the porosity have a good linear relationship, indicating that the decrease in the thermal conductivity along the vertical bedding is directly related to the generation of “cracks”. It can be seen in Figure 12b that the relationship between the thermal conductivity and the porosity along the parallel bedding decreases linearly, which is related to the “pyrolysis pores” formed after the pyrolysis of a large amount of organic matter in the oil shale under high-temperature conditions. However, the thermal conductivity coefficients do not continuously decrease linearly.

4.2. Application of the Experimental Results in Oil Shale Development Engineering

The thermal conductivity anisotropy of an oil shale affects the heat transfer range and heating efficiency of the oil shale strata. In order to quantify the thermal conductivity effect on the in situ electric heating pyrolysis of oil shale, the heat transfer range and the heating efficiency of electric heating pyrolysis technology of an oil shale ore bed by considering and not considering thermal conductivity anisotropy are analyzed through numerical calculation.

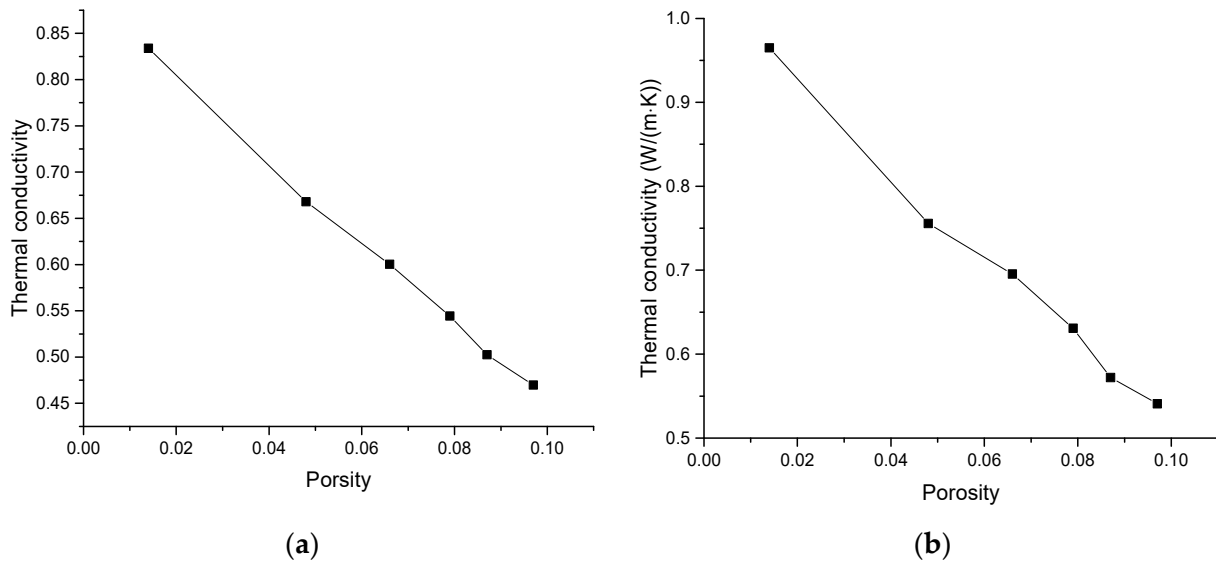


Figure 11. Relationship between thermal conductivity and porosity. (a) Perpendicular to bedding; (b) parallel to bedding.

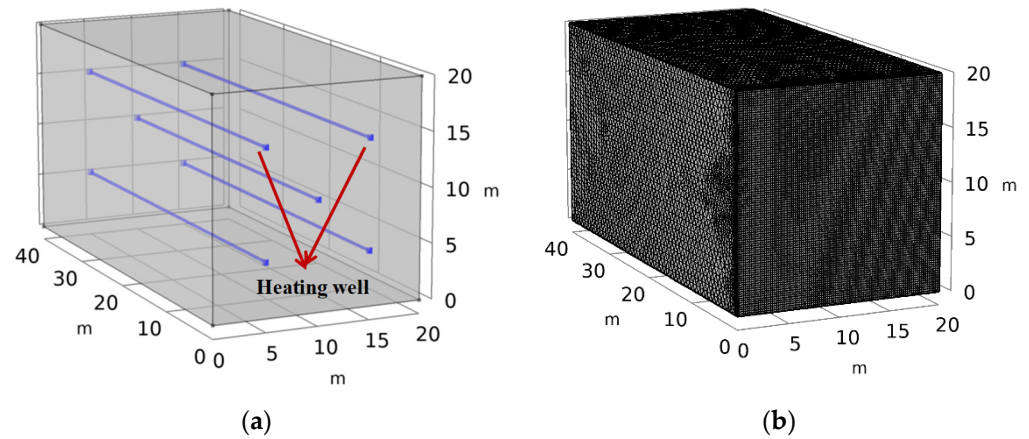


Figure 12. Geometric model and mesh. (a) Geometric model; (b) mesh.

Mathematical model [35]:

$$\rho_s c_p \frac{\partial T}{\partial t} - \text{div}(\lambda_s \nabla T) = 0 \quad (3)$$

where C_p is the specific heat capacity of the oil shale, ρ_s is the density of the oil shale, and λ_s is the thermal conductivity tensor of the oil shale.

$$\lambda_s = \begin{bmatrix} \lambda_{s-par} & 0 & 0 \\ 0 & \lambda_{s-par} & 0 \\ 0 & 0 & \lambda_{s-per} \end{bmatrix} \quad (4)$$

where λ_{s-par} is the thermal conductivity parallel to the direction of the oil shale bedding and λ_{s-per} is the thermal conductivity perpendicular to the direction of the oil shale bedding.

Geometric model:

The simulation area is a 20 × 40 × 20 m cube area. Five heating wells are located in the middle of the model, as shown in Figure 12a. Among them, the cube pyrolysis area uses three-dimensional tetrahedral units to divide the network, and the five heating wells use one-dimensional linear units to divide the network, as shown in Figure 12b, for a total of 132,415 tetrahedral networks.

Boundary conditions:

The constant temperature boundary of the heating well is $T = 600\text{ }^{\circ}\text{C}$ and the other boundaries are free boundaries, $T = T$.

Simulation results:

Figure 13 shows the distribution of the temperature field in the case of considering anisotropy and isotropy. It can be seen in the figure that, if heat conductivity anisotropy is considered, the cloud diagram of the temperature field distribution is elliptical. This is because the heat conduction coefficient in the parallel bedding direction is greater than that in the vertical bedding direction, resulting in the temperature conduction velocity in the parallel formation direction being greater than that in the vertical formation direction, further leading to the elliptical distribution of the temperature field. If heat conductivity isotropy is considered, the temperature field distribution will not be anisotropic and will be in a circular shape. In Han's study [36], the anisotropy of the thermal conductivity of oil shale is not considered and the distribution of temperature field is circular shape.

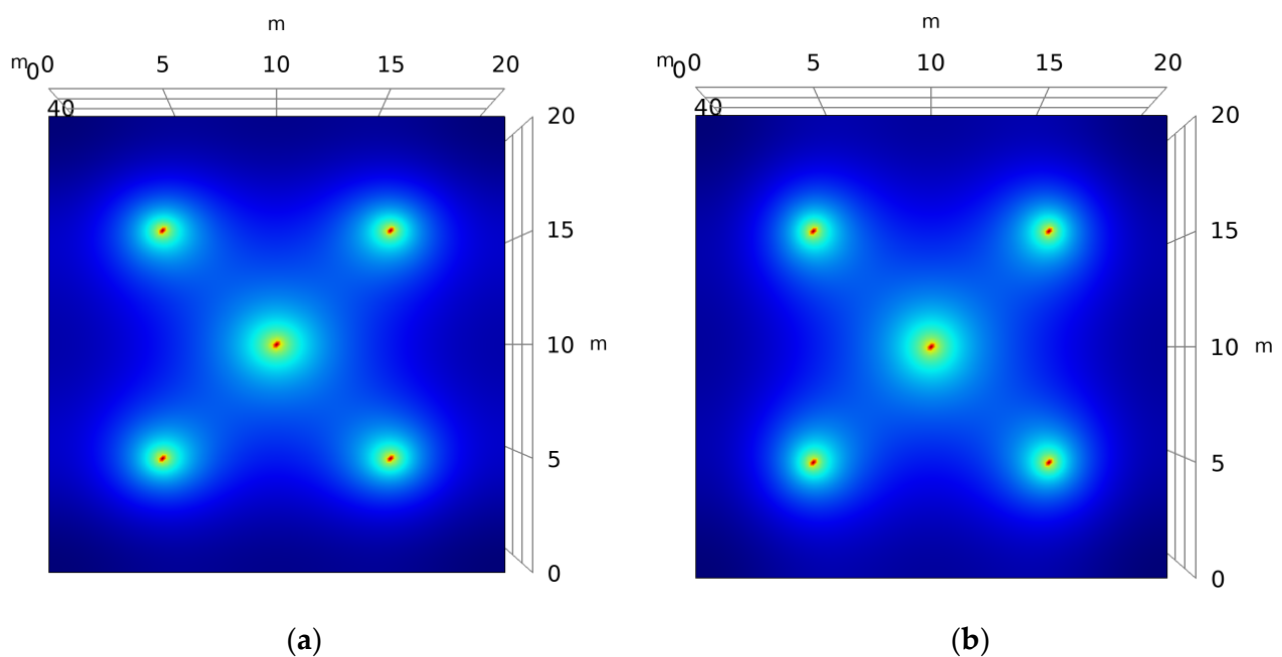


Figure 13. Temperature field distribution after heating for 1000D. (a) Considering anisotropy; (b) considering isotropy.

Figure 14 shows the variation of the average temperature of an oil shale ore bed with heating time when considering heat conductivity anisotropy and isotropy. It can be seen in the figure that under the condition of anisotropy, the temperature rise rate of the oil shale ore bed is smaller than that under the condition of isotropy. It can be seen that the thermal conductivity anisotropy affects the temperature conduction range and the heating efficiency of the oil shale ore bed. Yang [37] conducted a numerical study on the development of oil shale by in situ electric heating. The study found that it takes 9 years to complete the exploitation of oil shale in the corresponding area, which is similar to the research results in this paper and can verify the accuracy of the research results in this paper.

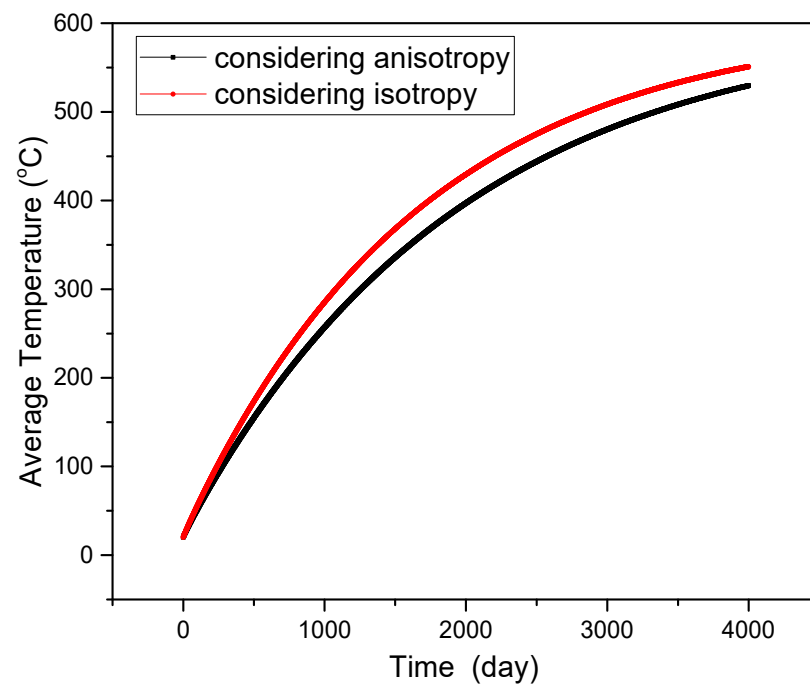


Figure 14. Variation of the oil shale reservoir's temperature with heating time.

5. Conclusions

In this study, the anisotropic pore and fracture structure of oil shale at different temperatures is obtained by CT scanning technology. The anisotropic thermal conductivity evolution of oil shale at high temperatures is studied using the hot disk method. The relationship between anisotropic thermal conductivity and anisotropic pore structure is analyzed and the following conclusions are obtained:

- (1) The thermal conductivity along the parallel bedding and the vertical bedding both decrease linearly with the increase in temperature, and the thermal conductivity along the parallel bedding is greater than that along the vertical bedding. The thermal conductivity ratio along the parallel bedding and the vertical bedding changes little with temperature.
- (2) The specific heat capacity first increases and then decreases with temperature and reaches its maximum at 400 °C. The reason why the maximum value is reached at 400 °C is that the pyrolysis of kerogen at 400 °C absorbs a lot of heat, resulting in the maximum specific heat capacity value being achieved.
- (3) The primary thermal conductivity anisotropy of oil shale is caused by sedimentary characteristics and natural fractures, while the change in the thermal conductivity anisotropy with temperature is caused by anisotropic thermal fractures.
- (4) The anisotropic thermal conductivity of oil shale affects the distribution of the temperature field and the heating efficiency of shale produced by electric heating. The temperature undergoes anisotropic conduction in the oil shale seam, and the cloud diagram of the temperature field distribution is elliptical.

Author Contributions: J.J.: Conceptualization; J.L.: methodology; W.J.: Software; W.C.: data curation; X.Z.: supervision. All authors have read and agreed to the published version of the manuscript.

Funding: The study on testing and evaluation of in situ stress and rock mechanical properties of low maturity shale oil reservoir, Project Number: 2019D-500806.

Institutional Review Board Statement: Not applicable.

Informed Consent Statement: Not applicable.

Data Availability Statement: Not applicable.

Acknowledgments: This study is supported by the study on testing and evaluation of in situ stress and rock mechanical properties of low maturity shale oil reservoir, Project Number: 2019D-500806, PetroChina RIPED.

Conflicts of Interest: The authors declare no conflict of interest.

Nomenclature

λ_{per}	Thermal conductivity in the direction of perpendicular to bedding
λ_{par}	Thermal conductivity in the direction of parallel to bedding
TG	Thermogravimetry
DTG	Differential thermogravimetric
ρ_s	The density of oil shale
C_p	Specific heat capacity of oil shale
λ_s	Thermal conductivity tensor of the oil shale

References

- Wang, J.; Feng, L.; Steve, M.; Tang, X.; Gail, T.E.; Mikael, H. China's unconventional oil: A review of its resources and outlook for long-term production. *Energy* **2015**, *82*, 31–42. [[CrossRef](#)]
- Sun, Y.; Bai, F.; Liu, B.; Liu, Y.; Guo, M.; Guo, W.; Wang, Q.; Lü, X.; Yang, F.; Yang, Y. Characterization of the oil shale products derived via topochemical reaction method. *Fuel* **2014**, *115*, 338–346. [[CrossRef](#)]
- Qing, W.; Hongpeng, L.; Baizhong, S.; Shaohua, L. Study on pyrolysis characteristics of huadian oil shale with isoconversional method. *Oil Shale* **2009**, *26*, 148–162. [[CrossRef](#)]
- Li, S.Y. The developments of Chinese oil shale activities. *Oil Shale* **2012**, *29*, 101–102. [[CrossRef](#)]
- Tissot, B.P.; Welte, D.H. *Petroleum Formation and Occurrence*; Springer: New York, NY, USA, 1984.
- Soone, J.; Doilov, S. Sustainable utilization of oil shale resources and comparison of contemporary technologies used for oil shale processing. *Oil Shale* **2003**, *20*, 311–323. [[CrossRef](#)]
- Jiang, X.M.; Han, X.X.; Cui, Z.G. New technology for the comprehensive utilization of Chinese oil shale resources. *Energy* **2007**, *32*, 772–777. [[CrossRef](#)]
- Kang, Z.; Zhao, Y.; Yang, D. Review of oil shale in-situ conversion technology. *Appl. Energy* **2020**, *269*, 115121. [[CrossRef](#)]
- Wang, L.; Zhao, Y.; Yang, D.; Kang, Z.; Zhao, J. Effect of pyrolysis on oil shale using superheated steam: A case study on the Fushun oil shale, China. *Fuel* **2019**, *253*, 1490–1498. [[CrossRef](#)]
- Kang, Z.; Zhao, Y.; Yang, D.; Tian, L.; Li, X. A pilot investigation of pyrolysis from oil and gas extraction from oil shale by in-situ superheated steam injection. *J. Pet. Sci. Eng.* **2020**, *186*, 106785. [[CrossRef](#)]
- Wang, L.; Yang, D.; Kang, Z. Evolution of permeability and mesostructure of oil shale exposed to high-temperature water vapor. *Fuel* **2021**, *290*, 119786. [[CrossRef](#)]
- Meijssen, T.; Emmen, J.; Fowler, T. In-situ oil shale development in Jordan through icp technology. In Proceedings of the Abu Dhabi International Petroleum Exhibition and Conference, Abu Dhabi, United Arab Emirates, 10–13 November 2014; OnePetro: Richardson, TX, USA, 2014.
- Looney, M.D. Chevron's plans for rubblization of greenriver formation oil shale (GROS) for chemical conversion. In Proceedings of the 31th Oil Shale Symposium, Golden, CO, USA, 17–21 October 2011.
- Alfarge, D.; Wei, M.; Bai, B. Factors affecting CO₂-EOR in shale-oil reservoirs: Numerical simulation study and pilot tests. *Energy Fuels* **2017**, *31*, 8462–8480. [[CrossRef](#)]
- Chinese Academy of Engineering (CAE). *Research on the Energy Development Strategy of China in Mid and Long-Term (2030 & 2050)*; Science Press: Beijing, China, 2011.
- Feng, L.Y.; Li, J.C.; Pang, X.Q. China's oil reserve forecast and analysis based on peak oil models. *Energy Policy* **2008**, *36*, 4149–4153. [[CrossRef](#)]
- Yang, D.; Wang, L.; Zhao, Y.; Kang, Z. Investigating pilot test of oil shale pyrolysis and oil and gas upgrading by water vapor injection. *J. Pet. Sci. Eng.* **2021**, *196*, 108101. [[CrossRef](#)]
- Gao, Q.; Tao, J.; Hu, J.; Yu, X. Laboratory study on the mechanical behaviors of an anisotropic shale rock. *J. Rock Mech. Geotech. Eng.* **2015**, *7*, 213–219. [[CrossRef](#)]
- Yang, S.; Yang, D.; Kang, Z. Experimental investigation of the anisotropic evolution of tensile strength of oil shale under real-time high-temperature conditions. *Nat. Resour. Res.* **2021**, *30*, 2513–2528. [[CrossRef](#)]
- Vernik, L.; Nur, A. Ultrasonic velocity and anisotropy of hydrocarbon source rocks. *Geophysics* **1992**, *57*, 727–735. [[CrossRef](#)]
- Vernik, L.; Landis, C. Elastic anisotropy of source rocks: Implications for hydrocarbon generation and primary migration. *AAPG Bull.* **1996**, *80*, 531–544.
- Vosteen, H.D.; Schellschmidt, R. Influence of temperature on thermal conductivity, thermal capacity and thermal diffusivity for different types of rock. *Phys. Chem. Earth Parts A/B/C* **2003**, *28*, 499–509. [[CrossRef](#)]
- Hajpál, M.; Török, A. Mineralogical and colour changes of quartz sandstones by heat. *Environ. Geol.* **2004**, *46*, 311–322. [[CrossRef](#)]

24. Brotons, V.; Tomás, R.; Ivorra, S.; Alarcón, J.C. Temperature influence on the physical and mechanical properties of a porous rock: San Julian's calcarenite. *Eng. Geol.* **2013**, *167*, 117–127. [[CrossRef](#)]
25. Wang, G.; Yang, D.; Zhao, Y.; Kang, Z.; Zhao, J.; Huang, X. Experimental investigation on anisotropic permeability and its relationship with anisotropic thermal cracking of oil shale under high temperature and triaxial stress. *Appl. Therm. Eng.* **2019**, *146*, 718–725. [[CrossRef](#)]
26. Wang, G.; Liu, S.; Yang, D.; Fu, M. Numerical study on the in-situ pyrolysis process of steeply dipping oil shale deposits by injecting superheated water steam: A case study on Jimsar oil shale in Xinjiang, China. *Energy* **2022**, *239*, 122182. [[CrossRef](#)]
27. Sun, Q.; Zhang, W.; Qian, H. Effects of high temperature thermal treatment on the physical properties of clay. *Environ. Earth Sci.* **2016**, *75*, 610. [[CrossRef](#)]
28. Li, Q. Temperature Field Simulation and Experiment of In-Situ Oil Shale Pyrolysis. Ph.D. Thesis, Jilin University, Changchun, China, 2012. (In Chinese).
29. Wang, L. Experiment and Simulation on Thermal Conductance During In Situ Oil Shale Mining by Electric Heating. Ph.D. Thesis, Jilin University, Changchun, China, 2014. (In Chinese).
30. Zhou, K.; Sun, Y.H.; Qiang, L.I.; Guo, W.; Lyu, S.D.; Han, J. Experimental research about thermogravimetric analysis and thermal physical properties of Nong'an oil shale. *Glob. Geol.* **2016**, *35*, 1178–1184.
31. Yu, Y.; Liang, W.; Bi, J.; Geng, Y.D.; Zhang, C.D.; Zhao, Y.S. Thermalphysical experiment and numerical simulation on thermal cracking of oil shale at high temperature. *Chin. J. Rock Mech. Eng.* **2015**, *34*, 1106–1115.
32. Kang, Z.; Yang, D.; Zhao, Y.; Hu, Y. Thermal cracking and corresponding permeability of Fushun oil shale. *Oil Shale* **2011**, *28*, 273. [[CrossRef](#)]
33. Saif, T.; Lin, Q.; Bijeljic, B.; Blunt, M.J. Microstructural imaging and characterization of oil shale before and after pyrolysis. *Fuel* **2017**, *197*, 562–574. [[CrossRef](#)]
34. Wang, G.; Yang, D.; Kang, Z.; Zhao, J. Anisotropy in thermal recovery of oil shale—Part 1: Thermal conductivity, wave velocity and crack propagation. *Energies* **2018**, *11*, 77. [[CrossRef](#)]
35. Wang, G.; Yang, D.; Kang, Z.; Zhao, J.; Lv, Y. Numerical investigation of the in situ oil shale pyrolysis process by superheated steam considering the anisotropy of the thermal, hydraulic, and mechanical characteristics of oil shale. *Energy Fuels* **2019**, *33*, 12236–12250. [[CrossRef](#)]
36. Hui, H.; Ning-Ning, Z.; Cai-Xia, H.; Yan, L.; Qing-Yong, L.; NA, D.; Xiao-Yan, H. Numerical simulation of in situ conversion of continental oil shale in Northeast China. *Oil Shale* **2016**, *33*, 45. [[CrossRef](#)]
37. Yang, D.; Zhao, J.; Kang, Z.Q.; Zhao, Y. Technology and numerical analysis of in-situ electrical heating on oil shale. *J. Liaoning Tech. Univ.* **2010**, *29*, 365–368.